nature nanotechnology

ARTICLES

PUBLISHED ONLINE: 9 MARCH 2015 | DOI: 10.1038/NNANO.2015.23

Plateau–Rayleigh crystal growth of periodic shells on one-dimensional substrates

Robert W. Day[1†], Max N. Mankin[1†], Ruixuan Gao[1], You-Shin No[2], Sun-Kyung Kim[3], David C. Bell[4,5], Hong-Gyu Park[2*] and Charles M. Lieber[1,5*]

The Plateau–Rayleigh instability was first proposed in the mid-1800s to describe how a column of water breaks apart into droplets to lower its surface tension. This instability was later generalized to account for the constant volume rearrangement of various one-dimensional liquid and solid materials. Here, we report a growth phenomenon that is unique to one-dimensional materials and exploits the underlying physics of the Plateau–Rayleigh instability. We term the phenomenon Plateau–Rayleigh crystal growth and demonstrate that it can be used to grow periodic shells on one-dimensional substrates. Specifically, we show that for certain conditions, depositing Si onto uniform-diameter Si cores, Ge onto Ge cores and Ge onto Si cores can generate diameter-modulated core–shell nanowires. Rational control of deposition conditions enables tuning of distinct morphological features, including diameter-modulation periodicity and amplitude and cross-sectional anisotropy. Our results suggest that surface energy reductions drive the formation of periodic shells, and that variation in kinetic terms and crystal facet energetics provide the means for tunability.

Controlling crystal growth at the nanoscale allows for command over both morphology and composition, thereby imparting enhanced or new functionality. For example, radial growth of conformal, crystalline shells over nanowire cores[1–4] provides a way to introduce unique electronic and optical characteristics to uniform-diameter core–shell nanomaterials[5–7]. Key physical phenomena, including optical absorption and electrical and thermal transport, are influenced by a nanowire's diameter[5,8], so it is interesting to consider whether diameter modulation can be introduced synthetically by design to generate material properties distinct from those of uniform-diameter nanowires. Several reports have been published on diameter-modulated nanowires synthesized by perturbing nanowire growth during axial elongation[9–16], by post-growth *ex situ* methods[17,18] and by strain-mediated core–shell heterostructure growth[19,20]. However, the ability of these techniques to simultaneously control multiple morphological features, tune these features over a wide range and combine cores and shells of arbitrary material composition remains limited.

Here, we report a general method of synthesizing diameter-modulated core–shell nanowires whose morphologies are tunable over an unprecedented range. We term this process 'Plateau–Rayleigh crystal growth', as it can be understood by considering the physics underlying the Plateau–Rayleigh (P–R) instability but in the context of nanowire crystalline shell growth. The P–R instability[21–26], first proposed in the 1800s to explain the break-up of a column of water into isolated droplets, more generally describes the constant-volume transformations of one-dimensional liquids and solids that reduce the total surface tension or energy. The relationships between *in situ* periodic shell growth by P–R crystal growth on a one-dimensional nanowire core versus conventional conformal shell growth and the P–R instability are shown schematically in Fig. 1a. Without a reactant, annealing nanowires at low pressures yields isolated nanocrystals[27–29], with a periodic spacing predetermined by the nanowire diameter due to the P–R instability. Here, by introducing reactant at low pressures, we reveal an unexplored growth regime, P–R crystal growth, where the diameter-modulation periodicity (pitch) and diameter-modulation amplitude (inner and outer diameters) are controlled for a given nanowire diameter.

Morphological tunability of diameter-modulated nanowires

We focus on Si periodic shell growth (see Methods and Supplementary Methods), because previous work has reported conformal Si shell growth over 100-nm-diameter Si cores under a wide range of experimental conditions[4,7], including temperatures between 650 and 850 °C with silane (SiH_4) as the Si shell source. In the absence of SiH_4, heating 100-nm-diameter Si nanowires at temperatures ≥775 °C leads to break-up into nanoparticles due to the P–R instability. At 900 °C this transformation occurs within 3 min (Fig. 1b), and much more slowly at lower temperatures (for example, >14 h at 775 °C), as expected[27–29]. Scanning electron microscopy (SEM) images (Fig. 1c) of nanowires produced following growth in the same temperature range (650–850 °C) but with SiH_4 and H_2 partial pressures ~10–100 times lower than for conventional conformal shell growth (see Methods and Supplementary Methods) highlight new features. First, the images show a periodic diameter modulation, where the pitch of the modulation varies as a function of specific growth conditions. Specifically, the periodic shell growth temperatures (in °C), SiH_4 flow rates (in s.c.c.m.) and partial pressures (in mtorr) for these images (top to bottom) were 775/0.3/1, 760/0.15/0.7, 800/0.8/4 and 775/1/5, respectively (Fig. 1c). Second, the periodic structure results from an additive process, because the inner/outer diameters of the modulations shown in the four images are all greater than the ~100 nm starting nanowire core diameter (280/490, 160/270, 170/320 and 180/330 nm). Furthermore, annealing 100 nm Si cores for ~2 h at a temperature similar to these growths (Supplementary Fig. 1)

[1]Department of Chemistry and Chemical Biology, Harvard University, Cambridge, Massachusetts 02138, USA. [2]Department of Physics, Korea University, Seoul 136-701, Republic of Korea. [3]Department of Applied Physics, Kyung Hee University, Gyeonggi-do 446-701, Republic of Korea. [4]Center for Nanoscale Systems, Harvard University, Cambridge, Massachusetts 02138, USA. [5]School of Engineering and Applied Sciences, Harvard University, Cambridge, Massachusetts 02138, USA. †These authors contributed equally to this work. *e-mail: hgpark@korea.ac.kr; cml@cmliris.harvard.edu

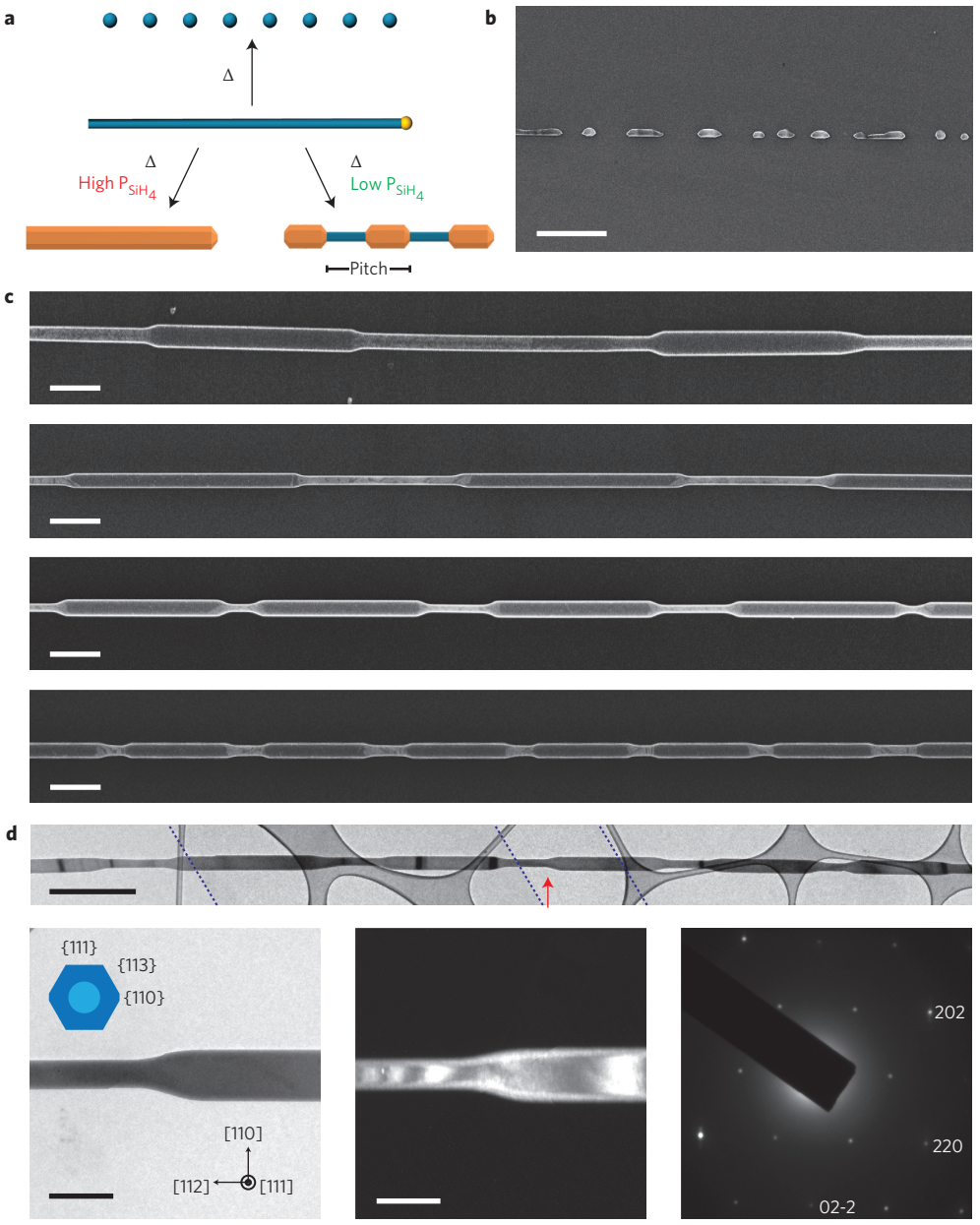

Figure 1 | Plateau–Rayleigh (P–R) crystal growth of periodic shell nanowires with tunable morphology. a, Schematic illustrating P–R instability, conformal shell growth and P–R crystal growth of periodic shells on nanowire cores at elevated temperatures. Pitch is defined as the sum of lengths of an inner and outer shell. **b**, SEM image of Si particles obtained after annealing 100 nm Si nanowire cores in vacuum at 900 °C for 3 min. Scale bar, 2 μm. **c**, Plan-view SEM images showing tunability of pitch from 2 to 12 μm for Si shells deposited on 100 nm Si nanowire cores. Growth conditions (temperature (°C), SiH_4 flow (s.c.c.m.), H_2 flow (s.c.c.m.), total pressure (torr), SiH_4 partial pressure (mtorr)) for images (top to bottom) were (775/0.3/180/0.61/1), (760/0.15/60/0.29/0.7), (800/0.8/60/0.29/4) and (775/1/60/0.29/5), respectively. Scale bars, 1 μm. **d**, Crystallographic characterization of Si periodic shell nanowires. Top: Composite bright-field TEM image of a Si periodic shell nanowire with average pitch of ~2.2 μm. The image consists of four individual low-magnification images stitched together. Image borders are indicated by dashed blue lines. Scale bar, 1 μm. Bottom left and middle: Bright- and dark-field TEM images from the area indicated by the red arrow. Scale bars, 400 nm. The dark-field TEM image was recorded using a {220} reflected beam. Inset: Schematic depicting the cross-sectional geometry and surface facet assignments of the periodic shell nanowires. Bottom right: Selected area electron diffraction patterns in the [111] zone axis from the region shown in the left and middle panels.

does not lead to any significant structural rearrangement of the core on the timescale relevant to periodic shell formation. Hence, these results show that the periodic shell structures arise from added SiH_4 as predicted by our P–R crystal growth concept. In addition, the yield of diameter-modulated nanowire structures is quite high, ~80–90%, as determined from optical and SEM images (Supplementary Fig. 2). Finally, control experiments in which the nanoparticle catalyst was removed by etching before shell growth (Supplementary Fig. 3) showed similar periodic structures and highlight that the observed modulation does not arise from diffusion of the metal catalyst along the nanowire core.

The structure and composition of these periodic shell nanowires have been characterized by transmission electron microscopy (TEM; see Methods and Supplementary Methods). A representative low-magnification TEM image (Fig. 1d) depicts a periodic shell nanowire with pitch of ~2 μm. Inspection of the interface between inner and outer shells by bright-field and dark-field imaging fails to indicate any defects observable in the [111] (Fig. 1d, left and

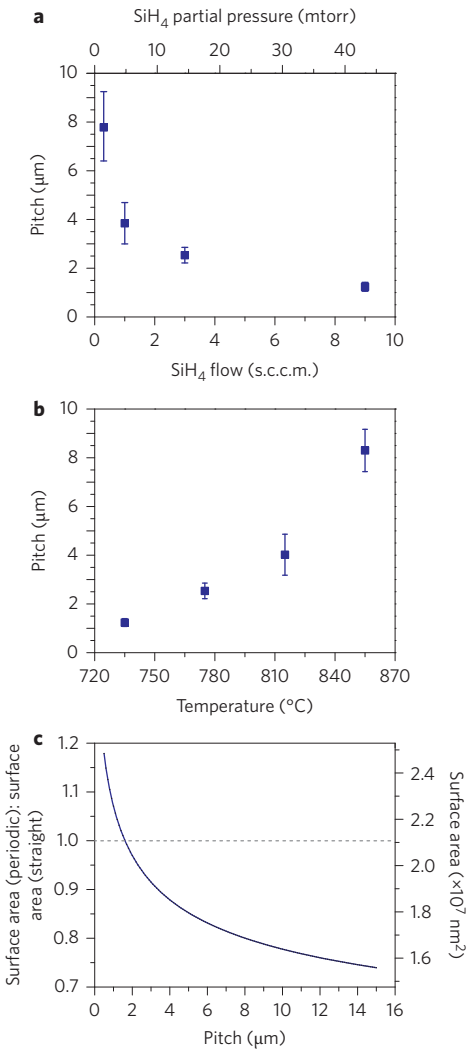

Figure 2 | Experimental synthetic control and model for P–R crystal growth. a, Dependence of pitch on SiH_4 flow rate/partial pressure. Si shells were deposited on 100 nm Si cores at 775 °C for variable SiH_4 flow rates (partial pressures) at a total pressure of ~0.3 torr. Error bars denote 1 s.d. from an average of ten nanowire measurements. SEM images of nanowires grown at variable SiH_4 flow rates are shown in Supplementary Fig. 7. **b**, Dependence of pitch on temperature. Si shells were deposited on 100 nm Si cores at variable temperature with a SiH_4 flow rate of 3 s.c.c.m. (SiH_4 partial pressure of 15 mtorr) at a total pressure of ~0.3 torr. Error bars denote 1 s.d. from an average of ten nanowire measurements. SEM images of nanowires grown at variable temperatures are shown in Supplementary Fig. 8. **c**, Surface area comparisons for variable pitch. The surface areas of periodic shell nanowires with various pitches are compared to a uniform-diameter (straight) nanowire with equivalent volume, as denoted by the dashed grey line. All structures have equivalent volume and the lowest possible surface-area configuration for a given pitch. Right axis: Absolute output values from the calculations assuming a total nanowire length of 30 μm, inner diameter of 100 nm and the pitch denoted on the bottom axis. Left axis: Dimensionless ratio of the surface area of a periodic shell nanowire to the surface area of a uniform-diameter core–shell nanowire of equivalent volume.

middle) and [110] (Supplementary Fig. 4) zone axes. Selected-area electron diffraction data obtained from different positions along the nanowire axis, including the inner and outer diameters of the modulation and interface between an inner/outer modulation, produced indistinguishable diffraction patterns; that is, the diffraction patterns all have a single set of spots in the [111] zone axis (Fig. 1d, right), indicating a [211] nanowire growth axis consistent with epitaxial, diameter-modulated growth and our previous work[4]. Elemental mapping by energy-dispersive X-ray spectroscopy (EDS; Supplementary Fig. 5) also confirmed that added material was Si, without appreciable impurities, showing that the nanowire composition is uniform along its axis within the 0.1–1% sensitivity of EDS. Together, TEM imaging, diffraction and compositional analyses demonstrate that the Si periodic shell nanowires are highly crystalline materials with clean core/shell interfaces and axial uniformity with respect to crystallography and composition.

To illuminate factors controlling the P–R crystal growth of periodic shells we explored growths where only time, SiH_4 flow rate or temperature was systematically changed. SEM images of periodic shell structures produced by varying the growth time from 0 to 8 min at 800 °C (SiH_4 flow = 0.8 s.c.c.m.; SiH_4 partial pressure = 4 mtorr; Supplementary Fig. 6) show the development of a diameter-modulated shell from a 100-nm-diameter Si nanowire. Analysis shows that the pitch, ~4.5 μm, does not change with time, although the diameters of the inner and outer shells increase as expected for this additive process. The diameter-modulation amplitude and outer shell fill ratio, which is defined as the ratio of outer shell length to the pitch, do change with time. Studies carried out with different SiH_4 flow rates at 775 °C and with other parameters constant (Fig. 2a and Supplementary Fig. 7) yielded systematic increases in average pitch: 1.2 ± 0.18, 2.5 ± 0.32, 3.8 ± 0.85 and 7.8 ± 1.42 μm (±1 standard deviation (s.d.), $N = 10$ for all measurements) for flow rates/SiH_4 partial pressures of 9/47, 3/15, 1/5 and 0.3/1 s.c.c.m./mtorr, respectively. Growths carried out at different temperatures with the SiH_4 flow rate and partial pressure (3 s.c.c.m./15 mtorr) and other parameters constant (Fig. 2b and Supplementary Fig. 8) produced average pitches of 1.2 ± 0.16, 2.5 ± 0.32, 4.0 ± 0.84 and 8.3 ± 0.87 μm (±1 s.d., $N = 10$ for all measurements) at growth temperatures of 735, 775, 815 and 855 °C, respectively. These studies show that the pitch can be systematically increased by increasing the temperature or decreasing the SiH_4 flow rate/partial pressure during growth.

P–R crystal growth model

To rationalize these experimental observations and explore the potential for synthetic design of new periodic structures, we considered a simple model for P–R crystal growth. Similar to P–R instability, where periodically spaced particles reduce the total surface energy compared to the original one-dimensional material, we assume that periodically spaced shells on a one-dimensional substrate reduce the total surface energy compared to a uniform-diameter nanowire of equivalent volume, thermodynamically driving growth of periodic shells over uniform-diameter shells. Moreover, we assume that longer-pitch nanowires have lower surface energies than shorter-pitch nanowires of equivalent volume. The kinetics of the growth, however, will determine (1) whether periodic (versus uniform-diameter) shells grow and (2) whether longer, lower-energy pitches develop. In the periodic shell growth regime (735–855 °C, ~0.1 torr), the diffusion length of adatoms is known to play a significant role in determining the final morphology and structure of Si films[30,31] (Supplementary Discussion). Thus, we hypothesize that Si adatom diffusion lengths are the most significant kinetic factor allowing access to lower-energy (that is, longer-pitch) periodic shell structures.

Our experimental results support the above model and highlight the implicit influence of kinetics for achieving lower-energy periodic configurations. First, Fig. 2a,b shows that lower SiH_4 flow rates/partial pressures and higher temperatures yield longer pitches, and corresponding thin-film studies have shown that lower precursor fluxes and higher temperatures are correlated with longer surface diffusion lengths[30]. Second, increasing only the H_2 partial

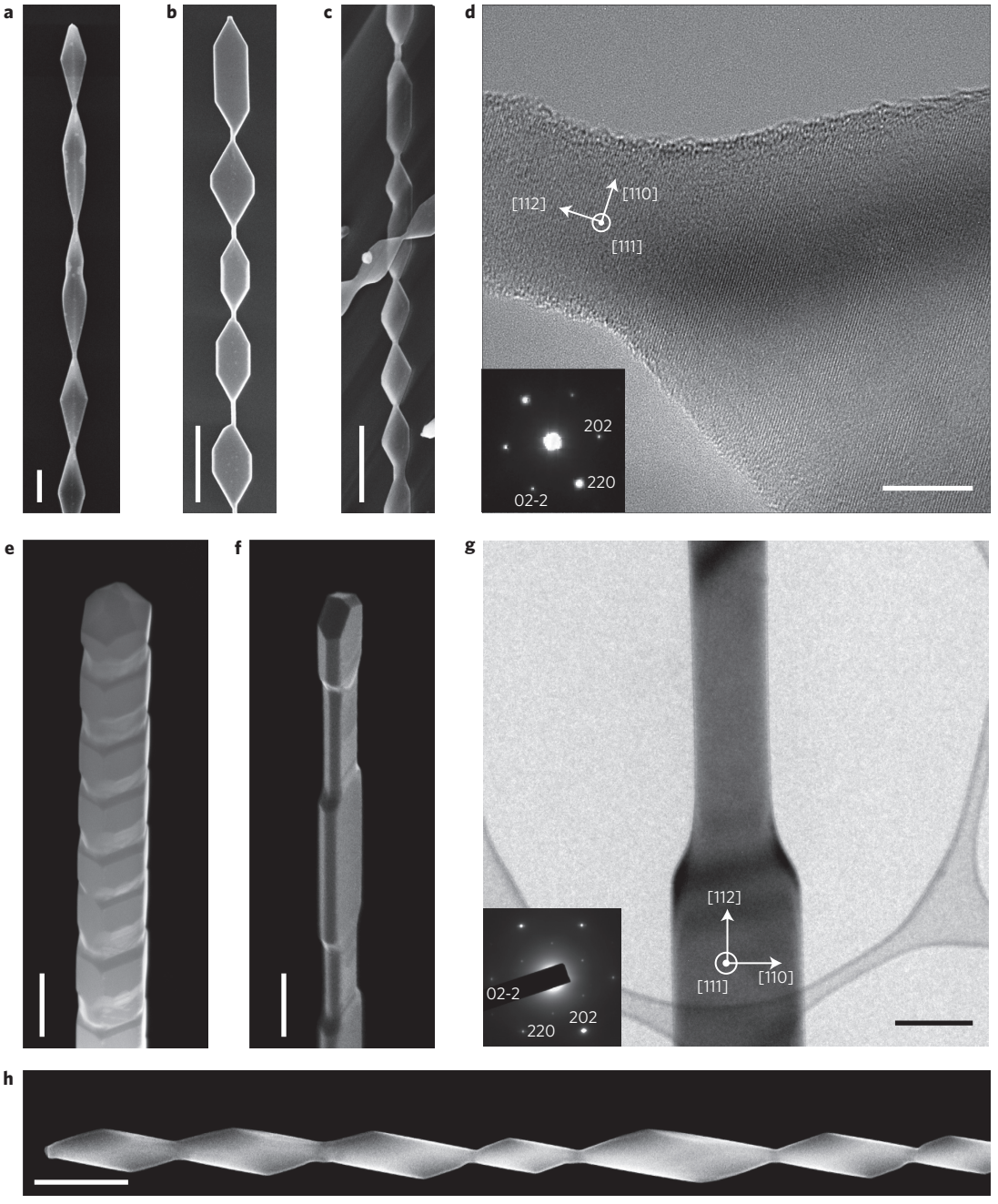

Figure 3 | Generality and scope of P–R crystal growth. a–d, Generality with respect to core diameter. SEM images of Si periodic shells deposited on Si nanowire cores with diameters of 50 nm (**a**), 30 nm (**b**), 20 nm (**c**). Scale bars, 400 nm. Si shells in **a** were deposited at 815 °C for 10 min with SiH_4 and H_2 flow rates of 0.3 s.c.c.m. and 60 s.c.c.m., respectively (SiH_4 partial pressure, 1 mtorr). In **b** and **c**, Si shells were deposited at 775 °C for 3 min with SiH_4 and H_2 flow rates of 3 s.c.c.m. and 200 s.c.c.m., respectively (SiH_4 partial pressure, 10 mtorr). **d**, High-resolution TEM image of the transition from inner to outer shell of a Si periodic shell grown on a 20 nm core nanowire. Scale bar, 10 nm. Inset: Selected area electron diffraction pattern in the [111] zone axis of the region of the nanowire shown in the TEM image. **e–g**, Synthetic control of aspect ratio. Head-on SEM images of low (~1) (**e**) and high (~4) (**f**) aspect ratio Si periodic shells grown on 100 nm Si nanowire cores. At 735 °C with a H_2 flow rate of 60 s.c.c.m., Si shells were deposited using SiH_4 flow rates/partial pressures of 3 s.c.c.m./15 mtorr for 5 min (**e**) and 0.3 s.c.c.m./1 mtorr for 22 min (**f**). Scale bars, 400 nm. TEM image (**g**) of the transition from inner to outer shell of a high (~4) aspect ratio Si periodic shell grown on a 100 nm core nanowire. Scale bar, 400 nm. Inset: Selected area electron diffraction pattern in the [111] zone axis of the region of the nanowire shown in the TEM image. **h**, Generality of P–R crystal growth with respect to material. SEM image of Ge periodic shells deposited on a Ge nanowire core with a diameter of 50 nm. Scale bar, 400 nm. Ge shells were deposited for 10 min at 470 °C followed by deposition for 3 min at 600 °C with GeH_4 flow rate/partial pressure of 40 s.c.c.m./20 mtorr.

pressure 100-fold but with a growth temperature and SiH_4 partial pressure that would otherwise produce periodic shells yields conformal shells. This result is consistent with the fact that surface diffusion lengths of Si adatoms are reduced by H_2 pressure[27]; that is, growth is kinetically trapped to yield higher-surface-energy conformal shells. Third, the introduction of PH_3 impurity leads to a reduction in periodic shell pitch from ~2.5 to 1.5 μm and ultimately conformal shells at higher PH_3 levels (Supplementary Fig. 9), consistent with decreased adatom surface diffusion lengths during Si film growth in the presence of PH_3 (ref. 32). Finally,

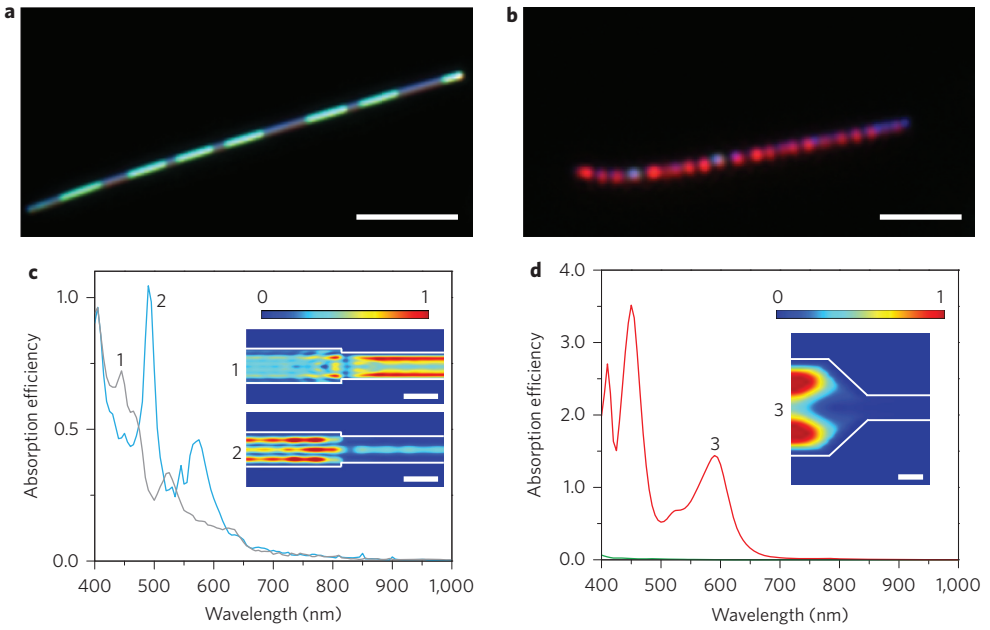

Figure 4 | Optical properties of Si periodic shell nanowires. a,b, Dark-field optical images of periodic shell nanowires with different dimensions. The dimensions, determined from SEM measurements, are D_{outer} = 260 and 150 nm, D_{inner} = 205 and 30 nm and pitch = 6 μm and 450 nm in **a** and **b**, respectively. Scale bars, 10 μm (**a**), 2 μm (**b**). **c,d**, Light absorption of inner versus outer shell modelled by FDTD simulations. Inner diameters, outer diameters and pitches of the nanowires in **a** and **b** were used as input dimensions for simulations in **c** and **d**, respectively. Outer aspect ratios were assumed to be 1.45 and 1.5 (H_{outer} = 180 and 100 nm) and inner aspect ratios were 1.15 and 1.0 (H_{inner} = 180 and 30 nm) for **c** and **d**, respectively. Spectra were obtained from finite-volume slices at the centre of the outer (blue and red) and inner (grey and green) shells (**c,d**). Insets: Normalized absorption mode profiles at wavelengths of 445 nm (top) and 490 nm (bottom), denoted by 1 and 2 in **c**, and at 590 nm, denoted by 3 in **d**. Scale bars, 250 nm (**c**) and 30 nm (**d**).

estimated diffusion lengths in the periodic shell growth regime range from 200 nm at lower temperatures to tens of micrometres at our highest growth temperatures (Supplementary Discussion) are consistent with the observed periodic shell pitch values.

Our model assumes that periodically spaced shells on a nanowire can have reduced surface energies compared to uniform-diameter core–shell nanowires of the same volume by reducing the total surface area and/or by elaboration of lower-energy surface facets. A straightforward geometric analysis (Supplementary Methods) allows us to test this assumption by directly comparing the ratio of surface areas for different periodic versus conformal shell configurations, given the general correspondence of surface area and surface energy[30,33]. For example, a periodic shell nanowire with a pitch of 3 μm, outer shell diameter of ~400 nm and inner shell of ~100 nm can have 92% of the surface area of a uniform-diameter nanowire with equivalent volume (Supplementary Fig. 10a). Similar calculations show that surface area decreases with increasing pitch as more of the Si volume becomes concentrated into fewer shells (Fig. 2c and Supplementary Fig. 10b). This latter trend is consistent with the experimental results described above, where conditions that increase the adatom diffusion length lead to longer pitch structures. We note that our model and geometric analysis are general, as they assume a cylindrical cross-section and isotropic surface energy densities.

We have also carried out calculations that explicitly consider the experimentally observed cross-sections and the corresponding energy densities for the different Si surface facets observed on our Si periodic shell structures (Supplementary Information and Supplementary Fig. 10c). Notably, these calculations show that our observed periodic shell nanowires have lower surface energies than uniform-diameter nanowires with equivalent volumes. Thus, the concepts and predictive trends of the model should be applicable to other material systems, sizes and cross-sectional geometries.

Generality and scope of P–R crystal growth

We explored the generality of P–R crystal growth through Si shell growth on different-diameter Si nanowire cores and the growth of other materials. SEM images of periodic Si shell structures from growth on Si nanowire cores with diameters of 50, 30 and 20 nm (Fig. 3a–c, respectively) highlight several points. First, these images demonstrate that P–R crystal growth yields periodic shell nanowires for a broad range of 'substrate' nanowire diameters. Second, these data show that pitches of periodic shells grown on smaller 30- and 20-nm-diameter nanowires can easily reach submicrometre dimensions with values of ~600 and ~330 nm, respectively. Third, these results demonstrate that periodic shell growth can yield substantial width-to-height anisotropy (addressed in more detail in the following). In addition, high-resolution, lattice-resolved TEM data obtained at the junction between one inner core and outer shell from a Si periodic shell grown on a 20-nm-diameter Si nanowire core (Fig. 3d) show continuous lattice fringes over the entire structure with no indications of defects or an interface between the core and shell. Selected area electron diffraction from this region (Fig. 3d, inset) yielded a single set of spots in the [111] zone axis. We note that the diffraction pattern and principle crystal directions of the nanowire core and shell are the same as those found for the larger low-aspect-ratio periodic shell structures obtained from P–R crystal growth on 100 nm Si nanowires (for example, Fig. 1d).

These diameter-dependent growth studies highlight a unique characteristic of P–R crystal growth—the capability to achieve substantial width-to-height anisotropy during periodic shell growth (Fig. 3a–c). We suggest that the inherent anisotropies in crystal facet surface energies[34] and adatom diffusion coefficients[31,35–37] enable synthetic tunability of aspect ratio. SEM images of structures resulting from P–R crystal growth on 100 nm Si nanowire cores under different conditions (Fig. 3e,f) show periodic shells with a

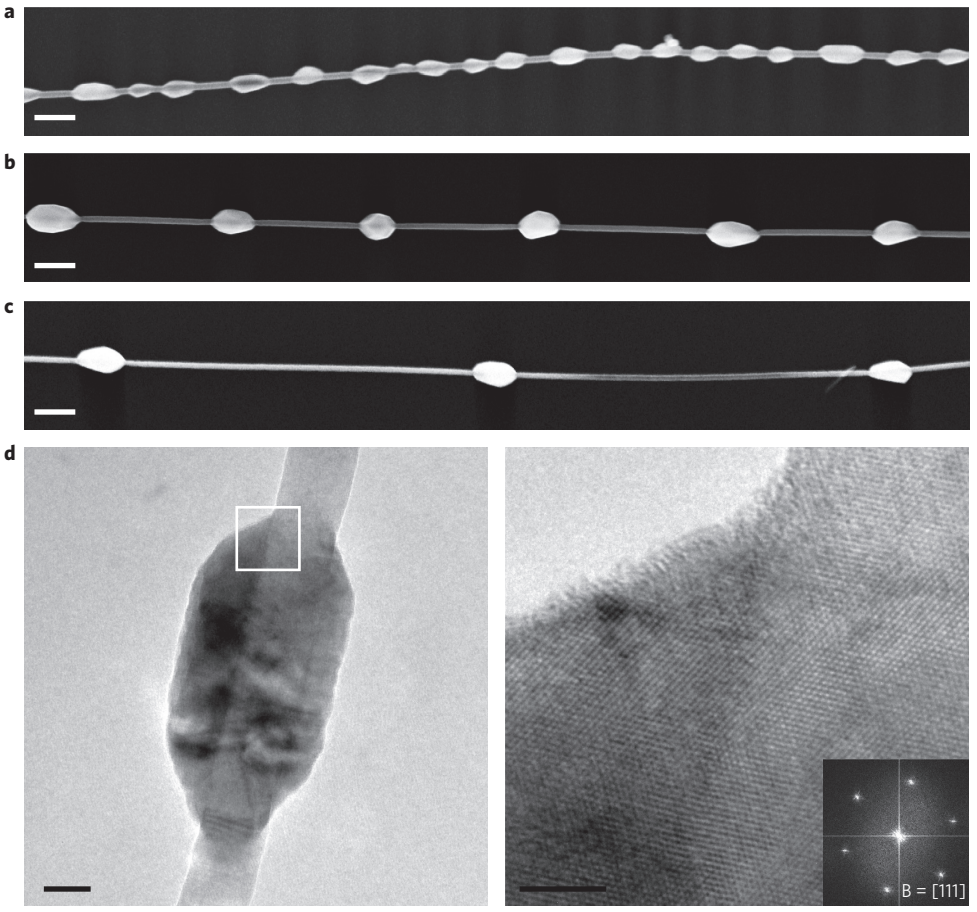

Figure 5 | P–R crystal growth of periodic shell heterostructures. a–c, SEM images of Ge periodic shells on Si nanowire cores with diameters of 30 nm. Ge was deposited at 520 °C with H_2 flow rate of 60 s.c.c.m. and GeH_4 flow rates/partial pressures of 40 s.c.c.m./16 mtorr (**a**), 8 s.c.c.m./4 mtorr (**b**) and 1 s.c.c.m./0.5 mtorr (**c**). Scale bars, 200 nm. **d**, Left: TEM image of a Si/Ge core/periodic shell nanowire with average pitch of ~500 nm. Scale bar, 20 nm. Right: High-resolution TEM image of the area indicated by the white box. Scale bar, 5 nm. Inset: FFT from core–shell region.

fourfold variation in cross-sectional anisotropy, supporting this idea. TEM images and electron diffraction data (Fig. 3g) further show that that the 4:1 anisotropy shell has the same structural quality and crystal directions as observed for periodic shell nanowires with 1:1 cross-sectional geometry (Fig. 1d) and periodic shell growth on 20 nm cores. Previous thin-film studies have reported net adatom diffusion from Si(111) to the Si(113) facets, elongating the (111) surface[31,37]. This is consistent with our work, where the higher-aspect-ratio structures, which have longer (111) surfaces, are observed with lower SiH_4 partial pressures and presumably longer diffusion lengths (Supplementary Fig. 11). Unlike pitch, the aspect ratio depends on the total growth time as well as temperature, preventing a more quantitative analysis at the moment. Future modelling that accounts for the differences in surface facet energies, anisotropic diffusion lengths and the ratio of the diffusion lengths to surface facet lengths should enable more controlled anisotropic periodic shell growth.

We also explored P–R crystal growth of Ge periodic shells on Ge cores. Deposition of Ge onto 50 nm Ge nanowire cores with GeH_4 partial pressures ~20 times lower than used for conformal Ge shell growth[1] yields periodic shell structures consistent with our model. An SEM image of a Ge periodic shell structure (Fig. 3h) grown at a GeH_4 partial pressure of 20 mtorr exhibits a pitch of 610 nm and an aspect ratio of ~1.5. Although P–R crystal growth of Ge periodic shell structures is more challenging than for Si, the fact that periodic Ge shells are obtained for a range of conditions (for example, 500–600 °C) suggests that the general concepts of surface energy minimization coupled with suitably long diffusion lengths will be applicable to the homoepitaxial growth of periodic shells on a wide range of one-dimensional materials.

Optical properties of diameter-modulated nanowires

One example of how P–R crystal growth can impart enhanced functionality is evident from the optical properties of diameter-modulated versus uniform-diameter nanowires[4,7,38]. A dark-field optical microscopy image of a 6-μm-pitch periodic structure with 205 nm inner and 260 nm outer diameters (Fig. 4a) shows a modulation in the colour of the scattered light coincident with the shell diameter modulation. The regions of different diameter efficiently scatter (and absorb) distinct wavelengths of light. In addition, a dark-field image of a much shorter ~450-nm-pitch periodic nanowire with 30 nm inner and 150 nm outer diameters (Fig. 4b; structural parameters determined from an SEM image of the same nanowire) shows a single scattering colour with the intensity maxima and modulation correlated with the outer diameter region and pitch, respectively.

To understand these images and the potential for controlling optical properties with periodic shell structures, we carried out finite-difference time-domain (FDTD) simulations (see Methods and Supplementary Methods). First, simulations of the absorption spectra for the long-period nanowire (Fig. 4c, dimensions from the nanowire in Fig. 4a) highlight the distinct absorption properties of the inner (grey) and outer (blue) shells. The absorption peaks found at distinct wavelengths for the inner and outer segments,

which give rise to the variation in colour observed in the dark-field image in Fig. 4a, correspond to resonant modes supported in these different-diameter regions. The optical resonant absorption mode profiles (Fig. 4c, inset) at 445 nm (denoted 1) and 490 nm (denoted 2) illustrate the spatially distinct light absorption in the inner versus outer shell. Second, simulations carried out for the short-period nanowire show that resonant absorption peaks are only observed for the larger outer diameter portion of the periodic structure, with little or no mode intensity sustained in the ~30-nm-diameter inner region (Fig. 4d, inset). Localized, spatially non-uniform axial absorption peaks are not observed for uniform-diameter Si nanowires. We suggest that these periodic shell nanowires structures could provide unique opportunities for optomechanical studies[39,40]. Specifically, their ability to sustain significant light confinement within the outer shells while having a reduced mass compared to uniform-diameter structures would be advantageous, as uniform-diameter nanowires with equivalent mass would be unable to support such optical confinement. Reducing the mass for optomechanics allows for higher mass detection limits[40,41] for resonator sensors and for probing quantum-limited mechanical motion and coherently cooling or amplifying the mechanical motion of resonators[39].

Finally, FDTD simulations were used to explore short-period structures where the inner region is sufficiently large to sustain resonant absorption modes. Interestingly, with the inner/outer dimensions of the periodic shell nanowire in Fig. 4a but with pitches <500 nm (Supplementary Fig. 12), high-amplitude peaks emerge at wavelengths >700 nm that can be assigned as coupled grating modes[42]. The calculated absorption efficiency for such a periodic shell nanowire is 0.7 at 929 nm, and bulk Si would require a thickness of ~50 μm to yield the same absorption efficiency. These results suggest that similar periodic shell nanowires with enhanced and tunable near-infrared absorption could be exploited for photodetectors and other optoelectronic devices. Furthermore, although lithography can impose grating structures in two dimensions, a unique advantage of P–R crystal growth is the capability to realize fully three-dimensional gratings with tunable anisotropy and, moreover, to prepare periodic shells on the vertical nanowire arrays currently being explored for solar energy conversion[3] and structural colour[43].

Diameter-modulated heterostructures and outlook

We have also explored the applicability of P–R crystal growth to the synthesis of core/periodic shell heterostructures. SEM images of a nanowire produced after introduction of GeH_4 at low pressures following the growth of 30-nm-diameter Si cores (Fig. 5a–c) clearly shows the growth of Ge periodic shells on Si cores. Growths at a fixed temperature of 520 °C with GeH_4 flow rates/partial pressures of 40 s.c.c.m./16 mtorr (Fig. 5a), 8 s.c.c.m./4 mtorr (Fig. 5b) and 1 s.c.c.m./0.5 mtorr (Fig. 5c) yielded periodic heterostructures with pitches of ~0.3, 0.9 and 2.4 μm, respectively. This observation of increasing pitch with decreasing reactant flow rate is consistent with the trend observed for Si periodic shell structures (Fig. 2a) and our model. A complete understanding of the energetics of the heterostructure growth will require consideration of other factors, including the relative energy densities of Si and Ge surfaces and the strain/interfacial energies[19,20]. In fact, it is likely that interfacial strain energy terms help to drive the formation of periodic shells, which is supported by the absence of Ge growth on the Si core between the Ge periodic shells (in contrast with our homoepitaxial Si/Si or Ge/Ge periodic shell structures), as observed in SEM (Fig. 5a–c) and TEM (Fig. 5d) images. Higher-resolution TEM images (Fig. 5d, right) and fast Fourier transform (FFT) analysis of the area suggest that the Ge shells are crystalline and grow epitaxially on the Si core, as indicated by the clear lattice fringes and two sets of related 'diffraction' spots in the FFT. To the best of our knowledge, our results are the first demonstration of pitch-controlled growth of radially conformal, Ge periodic shells on a Si core. The potential diversity of nanowire heterostructures combined with the empirical rules for P–R crystal growth demonstrated above suggest that periodic shell nanowire heterostructures represent a rich area for synthetic, physical measurement and theoretical exploration in the future.

In summary, we have presented a growth phenomenon that is fundamentally unique to one-dimensional materials: P–R crystal growth. Compared to previous reports of conformal shell growth, the deposition of shells at lower pressures and higher temperatures yields periodic shell structures for several core–shell material combinations, including Si on Si, Ge on Ge and Ge on Si, over a wide range of core diameters (20–100 nm). Tuning shell deposition conditions allows for a morphological control that is unprecedented compared to other synthetic methods with respect to both the range and number of controllable features (pitches from 400 nm to >12 μm, cross-sectional anisotropies from 1:1 to 4:1 and modulation amplitudes up to ~8:1). Our studies strongly suggest that periodic shell structures tend to minimize surface energy as long as lower-energy structures are kinetically accessible. The thermodynamic aspect of this model stems solely from a geometric consequence of adding volume to a one-dimensional structure and thus indicates a broad potential scope of P–R crystal growth, whereby periodic shells can reduce the surface area of a growing crystal irrespective of the size, material composition (for example, semiconductor, metal or dielectric) or origin of the one-dimensional substrate (vapour–liquid–solid (VLS) grown, top-down etched, and so on) and independent of the shell deposition process (chemical vapour deposition, solution-phase and similar). Thus, we expect our findings to have implications for material combinations and applications well beyond those mentioned here and, more generally, to illustrate the importance and opportunities in understanding the thermodynamics and kinetics unique to crystal growth on nanowires and other low-dimensional systems.

Methods

Si core nanowires were synthesized as described previously via the metal nanocluster-catalysed VLS mechanism[44]. Following core growth, the furnace temperature was ramped to 700–850 °C for periodic shell growth. At this temperature, shells were grown for 1–60 min at ~0.3 torr with gas flow rates of 0.15–10 s.c.c.m. SiH_4 and 0–200 s.c.c.m. H_2. For some syntheses, phosphine (PH_3; 1,000 ppm in H_2) was introduced to the reactor during shell growth at 0.5–20 s.c.c.m. flow rates. Ge core nanowires were typically synthesized from 50 nm Au catalysts at a total pressure of 300 torr with 200 s.c.c.m. H_2 and 20 s.c.c.m. germane (GeH_4; 10% in H_2) flow rates. Ge cores were nucleated for 5 min at 330 °C and grown for another 50 min at 270 °C. To grow Ge periodic shells, the temperature was increased to 450–600 °C and the pressure decreased to ~0.3 torr with GeH_4 flow rates of 20–40 s.c.c.m. End-on-view SEM images of periodic shell nanowires were recorded directly from the as-synthesized growth wafers. For plan-view SEM images and nanowire pitch measurements, nanowires were transferred to Si_3N_4-coated Si wafers. For TEM, scanning TEM (STEM) and electron diffraction analysis, nanowires were transferred to amorphous carbon-coated copper TEM grids. EDS maps were collected at a resolution of 512 × 400 using 400 ms dwell time per pixel in commercial EDAX Genesis software.

Received 1 July 2014; accepted 27 January 2015;
published online 9 March 2015

References

1. Lauhon, L. J., Gudiksen, M. S., Wang, D. & Lieber, C. M. Epitaxial core–shell and core–multi-shell nanowire heterostructures. *Nature* **420,** 57–61 (2002).
2. Heiss, M. *et al.* Self-assembled quantum dots in a nanowire system for quantum photonics. *Nature Mater.* **12,** 439–444 (2013).
3. Wallentin, J. *et al.* InP nanowire array solar cells achieving 13.8% efficiency by exceeding the ray optics limit. *Science* **339,** 1057–1060 (2013).
4. Kempa, T. J. *et al.* Coaxial multishell nanowires with high-quality electronic interfaces and tunable optical cavities for ultrathin photovoltaics. *Proc. Natl Acad. Sci. USA* **109,** 1407–1412 (2012).
5. Kempa, T. J., Day, R. W., Kim, S-K., Park, H-G. & Lieber, C. M. Semiconductor nanowires: a platform for exploring limits and concepts for nano-enabled solar cells. *Energy Environ. Sci.* **6,** 719–733 (2013).

6. De la Mata, M. *et al.* A review of MBE grown 0D, 1D and 2D quantum structures in a nanowire. *J. Mater. Chem. C* **1,** 4300–4312 (2013).
7. Kim, S-K. *et al.* Tuning light absorption in core/shell silicon nanowire photovoltaic devices through morphological design. *Nano Lett.* **12,** 4971–4976 (2012).
8. Hochbaum, A. I. *et al.* Enhanced thermoelectric performance of rough silicon nanowires. *Nature* **451,** 163–167 (2008).
9. Lim, S. K., Crawford, S., Haberfehlner, G. & Gradečak, S. Controlled modulation of diameter and composition along individual III–V nitride nanowires. *Nano Lett.* **13,** 331–336 (2013).
10. Musin, I. R., Boyuk, D. S. & Filler, M. A. Surface chemistry controlled diameter-modulated semiconductor nanowire superstructures. *J. Vac. Sci. Technol. B* **31,** 020603 (2013).
11. Hocevar, M. *et al.* Growth and optical properties of axial hybrid III–V/silicon nanowires. *Nature Commun.* **3,** 1266 (2012).
12. Hillerich, K. *et al.* Strategies to control morphology in hybrid group III–V/group IV heterostructure nanowires. *Nano Lett.* **13,** 903–908 (2013).
13. Givargizov, E. I. Periodic instability in whisker growth. *J. Cryst. Growth* **20,** 217–226 (1973).
14. Zhang, H. Z. *et al.* Dependence of the silicon nanowire diameter on ambient pressure. *Appl. Phys. Lett.* **73,** 3396 (1998).
15. Oliveira, D. S., Tizei, L. H. G., Ugarte, D. & Cotta, M. A. Spontaneous periodic diameter oscillations in InP nanowires: the role of interface instabilities. *Nano Lett.* **13,** 9–13 (2012).
16. Ma, Z. *et al.* Vapor–liquid–solid growth of serrated GaN nanowires: shape selection driven by kinetic frustration. *J. Mater. Chem. C* **1,** 7294–7302 (2013).
17. Christesen, J. D., Pinion, C. W., Grumstrup, E. M., Papanikolas, J. M. & Cahoon, J. F. Synthetically encoding 10 nm morphology in silicon nanowires. *Nano Lett.* **13,** 6281–6286 (2013).
18. Tian, J. *et al.* Boron carbide and silicon oxide hetero-nanonecklaces via temperature modulation. *Cryst. Growth Des.* **8,** 3160–3164 (2008).
19. Goldthorpe, I. A., Marshall, A. F. & McIntyre, P. C. Synthesis and strain relaxation of Ge-core/Si-shell nanowire arrays. *Nano Lett.* **8,** 4081–4086 (2008).
20. Schmidt, V., McIntyre, P. C. & Gosele, U. Morphological instability of misfit-strained core–shell nanowires. *Phys. Rev. B* **77,** 235302 (2008).
21. Plateau, J. A. F. Experimental and theoretical researches on the figures of equilibrium of a liquid mass withdrawn from the action of gravity. *Annu. Rep. Smithsonian Institution* 270–285 (1863).
22. Rayleigh, L. On the instability of jets. *Proc. London Math. Soc.* **10,** 4–13 (1878).
23. Eggers, J. Nonlinear dynamics and breakup of free-surface flows. *Rev. Mod. Phys.* **69,** 865–929 (1997).
24. Nichols, F. A. & Mullins, W. W. Surface- (interface-) and volume-diffusion contributions to morphological changes driven by capillarity. *Trans. Metall. Soc. AIME* **233,** 1840–1848 (1965).
25. Nichols, F. A. & Mullins, W. W. Morphological changes of a surface of revolution due to capillarity-induced surface diffusion. *J. Appl. Phys.* **36,** 1826–1835 (1965).
26. Nichols, F. A. On the spheroidization of rod-shaped particles of finite length. *J. Mater. Sci.* **11,** 1077–1082 (1976).
27. Barwicz, T., Cohen, G. M., Reuter, K. B., Bangsaruntip, S. & Sleight, J. W. Anisotropic capillary instability of silicon nanostructures under hydrogen anneal. *Appl. Phys. Lett.* **100,** 0931091–0931093 (2012).
28. Rauber, M., Muench, F., Toimil-Molares, M. E. & Ensinger, W. Thermal stability of electrodeposited platinum nanowires and morphological transformations at elevated temperatures. *Nanotechnology* **23,** 475710 (2012).
29. Peng, H. Y. *et al.* Bulk-quantity Si nanosphere chains prepared from semi-infinite length Si nanowires. *J. Appl. Phys.* **89,** 727 (2001).
30. Smith, D. L. *Thin-Film Deposition: Principles & Practice* Ch. 5 (McGraw-Hill, 1995).
31. Lim, S-H., Song, S., Park, T-S., Yoon, E. & Lee, J-H. Si adatom diffusion on Si (100) surface in selective epitaxial growth of Si. *J. Vac. Sci. Technol. B* **21,** 2388 (2003).
32. Fissel, A. & Richter, W. MBE growth kinetics of Si on heavily-doped Si(111):P: a self-surfactant effect. *Mater. Sci. Eng. B* **73,** 163–167 (2000).
33. Wulff, G. Zur frage der geschwindigkeit des wachstums und der auflösung der kristallflächen. *Z. Kristall. Mineral.* **34,** 449 (1901).
34. Lu, G-H., Huang, M., Cuma, M. & Liu, F. Relative stability of Si surfaces: a first-principles study. *Surf. Sci.* **588,** 61–70 (2005).
35. Mo, Y-W., Kleiner, J., Webb, M. B. & Lagally, M. G. Surface self-diffusion of Si on Si(001). *Surf. Sci.* **268,** 275–295 (1992).
36. Cho, K. & Kaxiras, E. Intermittent diffusion on the reconstructed Si(111) surface. *Europhys. Lett.* **39,** 287–292 (1997).
37. Xiang, Q. *et al.* Interfacet mass transport and facet evolution in selective epitaxial growth of Si by gas source molecular beam epitaxy. *J. Vac. Sci. Technol. B* **14,** 2381–2386 (1996).
38. Cao, L. *et al.* Engineering light absorption in semiconductor nanowire devices. *Nature Mater.* **8,** 643–647 (2009).
39. Gloppe, A. *et al.* Bidimensional nano-optomechanics and topological backaction in a non-conservative radiation force field. *Nature Nanotech.* **9,** 920–926 (2014).
40. Ramos, D. *et al.* Optomechanics with silicon nanowires by harnessing confined electromagnetic modes. *Nano Lett.* **12,** 932–937 (2012).
41. Tamayo, J., Kosaka, P. M., Ruz, J. J., Paulo, A. S. & Calleja, M. Biosensors based on nanomechanical systems. *Chem. Soc. Rev.* **42,** 1287–1311 (2013).
42. Yariv, A. & Yeh, P. *Photonics* (Oxford Univ. Press, 2006).
43. England, G. *et al.* Bioinspired micrograting arrays mimicking the reverse color diffraction elements evolved by the butterfly Pierella luna. *Proc. Natl Acad. Sci. USA* **111,** 15630–15634 (2014).
44. Cui, Y., Lauhon, L. J., Gudiksen, M. S., Wang, J. & Lieber, C. M. Diameter-controlled synthesis of single-crystal silicon nanowires. *Appl. Phys. Lett.* **78,** 2214–2216 (2001).

Acknowledgements

The authors thank A. Graham for assistance with electron microscopy. R.W.D. acknowledges a Graduate Research Fellowship from the National Science Foundation (NSF). M.N.M. acknowledges a Fannie and John Hertz Foundation Graduate Fellowship and an NSF Graduate Research Fellowship. R.G. acknowledges the support of a Japan Student Services Organization Graduate Research Fellowship. Y-S.N. acknowledges support for this work by the TJ Park Science Fellowship. C.M.L. acknowledges support of this research by a Department of Defense, National Security Science and Engineering Faculty Fellowships (N00244-09-1-0078) award and from Abengoa Solar New Technologies SA. H.-G.P. acknowledges support by the National Research Foundation of Korea (NRF) grant funded by the Korea government (MSIP) (no. 2009-0081565). S-K.K. acknowledges support of this work by the Basic Science Research Program through the NRF funded by the Ministry of Science, ICT & Future Planning (NRF-2013R1A1A1059423). This work was performed in part at the Center for Nanoscale Systems (CNS), a member of the National Nanotechnology Infrastructure Network (NNIN), which is supported by the NSF under award no. ECS-0335765. CNS is part of Harvard University.

Author contributions

R.W.D., M.N.M., H-G.P. and C.M.L. designed the experiments. R.W.D., M.N.M., R.G., Y-S.N. and S-K.K. performed the experiments. R.W.D., M.N.M. and C.M.L. wrote the manuscript. All authors discussed the results and commented on the manuscript.

Additional information

Supplementary information is available in the online version of the paper. Reprints and permissions information is available online at www.nature.com/reprints. Correspondence and requests for materials should be addressed to H.G.P. and C.M.L.

Competing financial interests

The authors declare no competing financial interests.